electricity

MDPI

Article

Procedure for Verifying Population Exposure Limits to the Magnetic Field from Double-Circuit Overhead Power Lines

Marco Landini [1], Giovanni Mazzanti [2,*] and Riccardo Mandrioli [2]

[1] Asset Department, AUSL Bologna, 40139 Bologna, Italy; mrc.landini@libero.it
[2] Department of Electrical, Electronic, and Information Engineering, University of Bologna, 40136 Bologna, Italy; riccardo.mandrioli4@unibo.it
* Correspondence: giovanni.mazzanti@unibo.it; Tel.: +39-051-209-3487

Abstract: The verification of the limits of the population's exposure to the magnetic field generated by double-circuit power lines from field measurements carried out on site is not trivial. It requires knowledge of the power line current instant values during the measurement period, the determination of the relationship between current and field at the measurement points (made more complex by the double-circuit overhead line configuration) and the use of that relationship to extrapolate the field values. Nevertheless, the verification of exposure limits for double-circuit power lines from on-site measurements is often conducted with rough, or not particularly stringent, procedures. A practical and straightforward procedure of general validity for non-optimized double-circuit lines is proposed here. No specific measurement position or conductors disposition knowledge is required as well as no complex three-dimensional finite element method code is necessary. The procedure, potentially also applicable to high- and extra-high-voltage lines, is validated on a medium-voltage (15 kV) double-circuit overhead power line study case. Exposure limits assessment suggests that if the line is operated at its rated capacity (230/285 A), the 3 μT quality target is missed. Results are provided with a 95% confidence interval ranging from ±100 nT to ±140 nT in all the cases.

Keywords: exposure limits; magnetic field; magnetic flux density; double-circuit line; overhead power line; multi-linear regression

Citation: Landini, M.; Mazzanti, G.; Mandrioli, R. Procedure for Verifying Population Exposure Limits to the Magnetic Field from Double-Circuit Overhead Power Lines. *Electricity* **2021**, *2*, 342–358. https://doi.org/10.3390/electricity2030021

Academic Editor: Pavlos S. Georgilakis

Received: 21 July 2021
Accepted: 6 September 2021
Published: 12 September 2021

1. Introduction

Electromagnetic fields (EMFs) produced by overhead power lines continue being among the topics collecting most of the attention from both specialized and the general public. Although low-frequency EMFs produced by overhead lines are classified as non-ionizing radiations incapable of producing mutagenic effects, their capability to induce biological tissue heating remains associated (without any solid and scientific-sounding evidence) with human health effects as cancer development [1,2]. This fear spreading in the general public was accentuated by a set of, now debunked, epidemiological studies which emphasized an alleged correlation between low-frequency EMF and childhood leukemia [3–7]. Together with human health-related concerns, there is a range of technical issues such as buried/overhead pipelines corrosion, all-dielectric self-supporting fiber optic cables failure, and railway signaling interference that can be reconducted to low-frequency EMF (mainly industrial frequency, i.e., 50/60 Hz) [1,3,8].

Policymakers have responded to EMF fear and issues with a set of regulations aiming to discipline EMF emissions (with a particular focus on magnetic fields) and, on the other hand, to compensate economic effects on the electrical assets and services [1,6,9,10]. Although European Union derived limiting values based on the International Commission on Non-Ionizing Radiation (ICNIRP) exposure limits (100 μT), member states might present more precautionary prescriptions [6,11]. Particularly relevant appear to be Slovenia and Italy, with quality targets for newly built facilities equal to 10 μT and 3 μT respectively [10,12,13]. The most restrictive values are applied in Switzerland in residential

area contexts where 1 μT is set as maximum exposure level [13]. Although the USA has not harmonized emission levels, New York State, where 20 μT limitations are applied at the edge of the overhead power line right of way, deserves to be mentioned [13]. American Conference of Governmental Industrial Hygienists recommends 1 mT as workers limiting values [10]. North Atlantic Treaty Organization (NATO) generally makes reference to the Institute of Electrical and Electronics Engineers (IEEE) limiting values (904 μT) set on the standard IEEE Std C95.1-2019 [10,14]. A broader list of emission limiting values involving a multitude of counties is reported in [10]. As mentioned above, together with the maximum exposure limit, certain countries (e.g., Slovenia, Italy, and Switzerland) require the verification of attention and quality levels. In most cases, both limits should be met considering the median value of the flux density around 24-h of a typical operation day. On the other hand, standard IEEE C95.1-2019 differentiates head/torso from limb exposure levels [14]. Since no universally recognized regulation and estimation procedure is available, flexible and straightforward approaches are necessary.

It stands clear that the assessment of the continuous exposure to low-frequency EMF is not a trivial procedure. Spot measurements lack representativeness, and more advanced estimations are required. Furthermore, power lines often present the so-called non-optimized double-circuit configuration where two independent lines share the same overhead corridor. In this kind of configuration, strongly unrelated currents might be involved, leading to difficult field determination. This topic produced plenty of scientific literary productions. The determination of Pareto optimal disposition of double-circuit conductors capable of optimizing EMF emission in overhead lines has been performed in [13]. In [15], the magnetic field generated by a 400 kV double-circuit transmission line in Poland has been calculated using superposition and reflection methods. However, a solid knowledge of each conductor disposition and the lack of lines independence hypothesis limit the applicability of the results to a well-confined scenario. In [16,17], the role of the current phase shift in the magnetic field calculation for non-optimized double-circuit power lines has been analyzed. In the case of phase shift, it appears evident that lack of knowledge (usually, rms only is recorded), assuming circuits in phase constitutes the most precautionary condition. In [18], the magnetic field spatial polarization pattern beneath the two circuits has been determined. Authors in [19] extended these results to complex configurations of power lines, including towers located on different heights as well as non-parallel spans. A comparison of field distribution in a compact and noncompact parallel line has been performed in [20], while the difference between a straight- and sagging-conductor geometrical approximation of double circuit overhead lines can be found in [21]. In [22], an assessment of the electric field induced by the overhead line magnetic field inside the human body in realistic postures has been performed. The analysis employed human models in live-line working positions over double-circuit four- and double-conductor bundle overhead transmission lines. Lunca et al. developed a LabVIEW (NI Corp.) program to compute the magnetic field of single- and double-circuit overhead lines, referring to Romania's transmission towers shape [23]. The magnetic field in double-circuit twisted three-phase cables has been determined and used as a tool for fault detection [24,25]. Finally, sheath standing voltage induced by double-circuit overhead lines on underground cables sharing the same right of way has been studied in [26]. Even in sheath cross-bonding and phase transposition, the longer the parallel corridor is, the higher the induced voltage is.

To the best of the Authors' knowledge, no straightforward flux density estimation procedure capable of assessing in a prudent way exposure with minimum information is available yet. This paper proposes a magnetic field calculation procedure for double-circuit overhead powerlines requiring the sole knowledge of on-site field measurements (spanning over a representative amount of time) and the corresponding line currents (provided by the system operator). Unlike most of the contributions mentioned above, no specific measurement position or conductors disposition knowledge is required. Current in the two circuits could be strongly unrelated with the sole assumption to consider them

balanced and in phase between each other. A relationship between reference currents and arbitrary positions (far enough from the line) is found utilizing a straightforward and widely employed multi-linear regression based on the least squares. The regression coefficient can be used for determining the exposure in a particularly flexible way according to the in-force regulation. For instance, the maximum magnetic field can be assessed assuming as reference current the maximum thermal capability of the line. At the same time, the quality target can be evaluated referring to the median current. The procedure is designed specifically for non-optimized double-circuit lines, but it could also be applied to two parallel single-circuit lines. Although the validation is carried out using a medium voltage scenario, the principle could be applied effortlessly also to high- and extra-high-voltage overhead lines. Outcome's uncertainty is assessed assuming that no measurements accuracy information is available. All error sources are accounted for implicitly without introducing clunky formulations. No need for three-dimensional finite element method (FEM) codes is necessary. All assumptions and simplifications are discussed, and hints for the overcome of method limitations are given. No specific term capable of considering possible strong field sources not proportional to the line currents is introduced.

In Section 2, background on the magnetic field calculation is provided. In Section 3, the proposed calculation procedure is described. Validation on a real medium-voltage scenario is performed in Section 4. Finally, Section 5 concludes the paper.

2. Calculation of Exposure to the Magnetic Field Generated by Power Lines

A power line can be approximated as a set of conductors with positions imposed by the size and height of the towers. The calculation of the magnetic field H, as well as magnetic flux density B in the area adjacent to the line, can be conducted using the integration of the differential Biot-Savart law. The latter can be simplified adopting the assumption reported in the CEI 211-4:2008 and ISO 17.220.20 technical standards [27,28]:

1. Infinite plane terrain having a relative permeability $\mu_r = 1$;
2. line conductors, straight, parallel, and having infinite length;
3. balanced set of line currents.

In particular, by adopting a two-dimensional cartesian coordinate system xy orthogonal to the line axis, the magnetic flux density vector B relative to a generic time instant t and a point in space P identified by a vector having coordinates x_P and y_P can be divided into its scalar components, as follows:

$$B_x(P,t) = \frac{\mu_0}{\pi\sqrt{2}} \sum_{k=1}^{M} \frac{I_k \sin\left[\omega t - \Delta_k - 2(k-1)\frac{\pi}{3}\right](y_k - y_P)}{(x_k - x_P)^2 + (y_k - y_P)^2} \quad (1)$$

$$B_y(P,t) = \frac{\mu_0}{\pi\sqrt{2}} \sum_{k=1}^{M} \frac{I_k \sin\left[\omega t - \Delta_k - 2(k-1)\frac{\pi}{3}\right](x_k - x_P)}{(x_k - x_P)^2 + (y_k - y_P)^2} \quad (2)$$

where μ_0 is the vacuum magnetic permeability, ω is the grid angular frequency, M is equal to 3 or 6 in case of single- or double-circuit line, respectively. I_k is the rms value of the k-th current flowing into the wire located at coordinates x_k and y_k. Conductors enumerated with $k = 1, 2, 3$ are forming circuit A, while conductors identified with $k = 4, 5, 6$ form circuit B. Angle Δ_k is set equal to 0 or $\Delta\varphi$ whether k is part of circuit A or B, respectively.

2.1. Single-Circuit Lines

In the case of single-circuit line, it can be seen that rms values of Equations (1) and (2) are proportional to the line current as (referring to circuit A) [29]:

$$B_x(P) = K_{Px} I_A \quad (3)$$

$$B_y(P) = K_{Py} I_A \quad (4)$$

where K_{Px} and K_{Py} are appropriate proportionality coefficients derived from Equations (1) and (2). The magnetic induction rms value evaluated in the point P can be computed as:

$$B_P = \sqrt{[B_x(P)]^2 + [B_y(P)]^2} = I_A \sqrt{{K_{Px}}^2 + {K_{Py}}^2} = K_{PA} I_A \tag{5}$$

2.2. Double-Circuit Lines

For a double circuit line, on the other hand, it is easy to verify that if $\Delta\varphi = 0$, as in non-optimized lines [29,30], rms values of Equations (1) and (2) can be calculated as:

$$B_x(P) = B_{Ax}(P) + B_{Bx}(P) \tag{6}$$

$$B_y(P) = B_{Ay}(P) + B_{By}(P) \tag{7}$$

In this case, B_P may be derived as follows:

$$\begin{aligned} B_P &= \sqrt{[B_x(P)]^2 + [B_y(P)]^2} \\ &= \sqrt{[B_A(P)\cos\theta_1 + B_B(P)\cos\theta_2]^2 + [B_A(P)\sin\theta_1 + B_B(P)\sin\theta_2]^2} \end{aligned} \tag{8}$$

where θ_1 and θ_2 are the spatial orientation of vectors $B_A(P)$ and $B_B(P)$. In case of $\theta_1 = \theta_2 = \theta$ (if the point P is far enough from the line), Equation (8) becomes:

$$\begin{aligned} B_P &= \sqrt{[B_x(P)]^2 + [B_y(P)]^2} \\ &= \sqrt{[B_A(P) + B_B(P)]^2 \cos^2\theta + [B_A(P) + B_B(P)]^2 \sin^2\theta} = B_A(P) + B_B(P) \\ &= K_{PA} I_A + K_{PB} I_B \end{aligned} \tag{9}$$

Equation (9) shows that, under the simplifications above, the total field is expressed as a bilinear combination of the currents of each circuit. As visible, to perform the calculation of B_P a priori knowledge of line currents is necessary. Once proportional factors K_{PA} and K_{PB} are determined, the field produced by an arbitrary reference current can be derived easily [12]. A novel calculation procedure of these factors is discussed in the next Section.

When the above assumptions and simplifications cease to be valid, it may be appropriate to use calculation codes like the 3D FEM [27,28,30,31].

3. Proposed Calculation Procedure

As shown above, measuring the magnetic field in a given point in space and knowing the corresponding current value makes it possible to determine the proportionality constant between field and current. Then measured field value corresponding to an arbitrary reference current can be determined.

Since the instant value of the magnetic flux density B depends on the instant currents, simply measuring the field does not provide enough information about the exposure that a receiver could experience. It is necessary to correlate field measurement with a current line load diagram (the system operator must store representative current rms samples). Moreover, a spot measurement is not sufficient; the uncertainty inherent in measurement methods and the possible presence of other independent low-frequency EMF sources make the determination of the proportionality constant a not trivial procedure. Therefore, it is appropriate to acquire the magnetic flux density values over an appropriate duration period, representative of the regular service conditions of the line, to determine the proportionality constant between field and current with as little uncertainty as possible.

3.1. Single-Circuit Lines

In the case of a single-circuit power line (indicated as circuit A), by measuring n field values B_{Pi} over an appropriate time interval and by acquiring current I_{Ai} from the line load diagram, it is possible to estimate the coefficient of proportionality K_{PA} accurately.

The simplest way to compute the coefficient is through the mean of the ratio between each i-th field and current:

$$K_{PA} = \frac{1}{n}\sum_{i=1}^{n}\frac{B_{Pi}}{I_{Ai}} \tag{10}$$

As visible in Equation (11), the coefficient K_{PA} determines the reference induction value B_r corresponding to an appropriate reference current I_r opening to a fair comparison with grid codes, standards, and quality benchmarks [1,6,10–14]. Both maximum and quality limiting levels can be assessed.

$$B_r = K_{PA} I_r \tag{11}$$

3.2. Double-Circuit Lines

In the case of double-circuit power lines, as stated above, the two currents, although supposedly balanced, are generally characterized by a mutual angle shift $\Delta\varphi$ (see Equations (1) and (2)) and by a mutual spatial mismatch θ, (see Equations (8) and (9)). Therefore, each circuit generates a magnetic flux density vector with its spatial components and its electrical phase—the total field results from the vectorial composition of each circuit field. The worst case is when the two vectors have the same electrical phase and the same spatial disposition (i.e., they are in phase and parallel) so that the total field is obtained by simply adding the modules of the two vectors [16,17]. Therefore, in the following developments, assumptions $\Delta\varphi = 0$ and $\theta = 0$ hold.

Under these precautionary hypotheses, in a generic point P (not too close to the conductors), it is possible to utilize Equation (9). As reported in Equations (12) and (13), the proportionality coefficients are defined as the ratio between the field in the measurement point and the individual line current.

$$K_{PA} = \frac{B_P}{I_A} \quad \text{having} \quad I_B = 0 \tag{12}$$

$$K_{PB} = \frac{B_P}{I_B} \quad \text{having} \quad I_A = 0 \tag{13}$$

A novel procedure is necessary since it is particularly complicated to evaluate these coefficients assuming only one working circuit.

The procedure for estimating K_{PA} and K_{PB} proposed in this work is obtained from the numerical processing of the data vectors of the values of $B_P(k)$ (obtained by measurements in the location under test for a representative amount of time) and the values of currents $I_A(k)$ and $I_B(k)$ (communicated by the operator of the power line) through a multiple linear regression procedure based on the method of the linear least squares. According to this procedure, K_{PA} and K_{PB} represent the coefficients of the regression plane equation. This method is widely recognized as a good estimator of linear distribution as the one here treated. A multiple linear regression always presents a closed-form solution easily computable using the formulation:

$$\begin{bmatrix} K_{PA} \\ K_{PB} \end{bmatrix} = \left([X]^T[X]\right)^{-1}[X]^T[Y] \quad \text{having} \quad \begin{cases} [X] = \begin{bmatrix} I_A(k) & I_B\ (k) \end{bmatrix} \\ [Y] = [B_P(k)] \end{cases} \tag{14}$$

where $B_P(k)$, $I_A(k)$, and $I_B(k)$ are three $k \times 1$ column vectors containing sampled data.

Since the system presents two unknown variables and several equations (one for each triplet of samples), the regression procedure produces a residual term ε. In the vast majority of the cases, the number of samples is high enough for stating that the residuals are represented by a random variable ε having a normal distribution with a null expected value and standard error σ_ε. The latter accounts for the measurement uncertainty and the random processes that always characterize on-field measurement procedures. However, also regressors K_{PA} and K_{PB} present a certain grade of uncertainty that all main statistical tools (e.g., MATLAB, LabVIEW, Python, R, Julia, Octave, and so on) provide under the

form of confidence intervals (usually 95%) or standard deviation ($\sigma_{K_{PA}}$ and $\sigma_{K_{PB}}$). These can be computed as:

$$\begin{bmatrix} \sigma^2_{K_{PA}} & - \\ - & \sigma^2_{K_{PB}} \end{bmatrix} = \sigma^2_{\varepsilon}\left([X]^T[X]\right)^{-1} \quad \text{having} \quad \begin{cases} [X] = \begin{bmatrix} I_A(k) & I_B & (k) \end{bmatrix} \\ [Y] = [B_P(k)] \end{cases} \tag{15}$$

These terms can be used for computing the total variance as:

$$\sigma^2_{B_{rP}}(I_{rA}, I_{rB}) = \sigma^2_{K_{PA}}\left[{I_{rA}}^2 - 2I_{rA}\bar{I}_A + 2\,{\bar{I}_A}^2\right] + \sigma^2_{K_{PB}}\left[{I_{rB}}^2 - 2I_{rB}\bar{I}_B + 2\,{\bar{I}_B}^2\right] + \sigma^2_{\varepsilon} \approx \sigma^2_{\varepsilon} \tag{16}$$

where $\bar{I}_A$ and $\bar{I}_B$ are the mean values of the current samples used for the regression. The variance changes as a function of the current couple (I_{rA}; I_{rB}) and its minimum is located at ($\bar{I}_A$; $\bar{I}_B$). As visible, the calculation is rather bulky and requires the knowledge of the current means. Often nonconstant contributions due to $\sigma_{K_{PA}}$ and $\sigma_{K_{PB}}$ are negligible in comparison to σ_{ε}, leading to a substantial simplification of the confidence interval evaluation. The latter statement ceases to be valid if (I_{rA}; I_{rB}) is evaluated far from ($\bar{I}_A$; $\bar{I}_B$).

These coefficients, which depend on the point of measure P, as well as of course on the circuit under consideration, allow estimating the reference induction value B_r corresponding to appropriate current reference values I_{rA} and I_{rB} (which might even be noticeably different), according to:

$$B_{rP} = B_{rP}(I_{rA}, I_{rB}) = K_{PA}I_{rA} + K_{PB}I_{rB} \tag{17}$$

3.3. Procedure Sum up and Discussion

The above-described method is here reassumed and discussed. In particular, Figure 1 summarizes the procedure using a flowchart. The latter will be used in Section 4 for the validation of the proposal. Figure 1 reports the case in which the magnetic field of a double-circuit line is characterized; a similar procedure could be applied to a single-circuit case through Section 3.1 considerations.

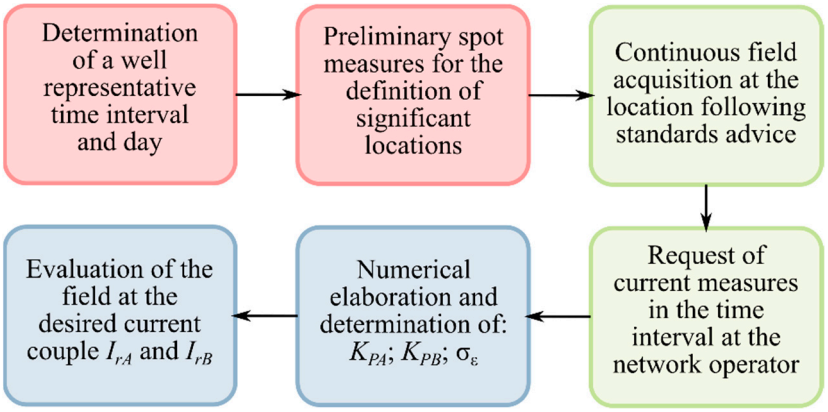

Figure 1. Flowchart of the proposed procedure applied to a double-circuit line—preliminary steps in red, data acquisition in green, and numerical post-processing in blue.

The multiple linear regression evaluated with the least squares method has been chosen for many reasons. Firstly, as shown in Equation (9), the paper deals with a linear problem, and therefore linear fitting methods should be preferred. Secondly, multiple linear regression is remarkably straightforward because available with high-level functions in almost all the main numerical tools and however still implementable at a low level with a simple formulation (see Equation (14)). Furthermore, the uncertainty of the measurements is considered implicitly. This limits the cumbersomeness of the method, and it is beneficial when the transmission system operator does not provide an adequate characterization of the phasor measurement unit (PMU) used. Finally, it is the de-facto standard when

linear data fitting is required. Its analysis of variance (ANOVA) can be performed through a widely recognized collection of statistical tools that permit a good understanding and evaluation of the outcomes.

Possible Extensions of the Proposed Method

As evident, the current development aims at providing a procedure that does not require cumbersome analytical tools. In this regard, a single-circuit line procedure can be implemented utilizing a simple arithmetic mean. However, one could extend the least-squares methodology shown in the double-circuit line case to fit the single-circuit line one by properly reshaping the design matrix $[X]$. Although some degree of precision can be gained, the procedure becomes more complicated.

Similarly, more complex structures involving more than two circuits (distribution and transmission corridors with multiple parallel overhead lines) could be investigated. This extension could theoretically be achieved by extending the design matrix $[X]$ to accommodate more current samples at the expense of the result variance that could noticeably increase.

To guarantee procedure ease, the measurement accuracy is not directly involved, and it is numerically accounted inside the variance of proportionality coefficients and residuals. As it will be apparent in Section 4, this rather firm simplification provides valid results as long as the measurements present an acceptable level of accuracy and are performed under representative conditions of the normal operation of the lines. However, the current methodology based on multiple linear regression and the least squares could be generalized employing the total least square modeling procedure capable of explicitly considering observational errors in both dependent (B_P) and independent (I_A and I_B) variables directly during the regression rather than implicitly as here performed. This procedure is at the base of the so-called Deming regression and orthogonal regression.

At the current stage, no specific term dedicated to taking into account strong field sources not proportional to the line currents is introduced. Future studies might amend the design matrix $[X]$ aiming at filling this limitation in case of impactful errors.

These more complicated methods and possible extensions are outside the paper's scope, and no further detail is provided here.

4. Validation of the Proposed Method on a Medium Voltage Double-Circuit Line

4.1. Building under Test

The area of interest (see Figure 2) houses a residential building (highlighted in yellow), for which an exposure assessment must be carried out.

The following low-frequency EMF sources are present in the surrounding area:

- Medium voltage (15 kV) double-circuit overhead power line adjacent to the building under consideration (see Figure 2), which is the primary field source, consisting of circuit A (displayed in blue color) and circuit B (displayed in orange color);
- Nearby distribution substation (not displayed);
- Three further medium-voltage lines are derived from the distribution substation.

Circuit A and circuit B have the following characteristics:

- Circuit A: overhead power line with a conductor section of 70 mm^2 and thermal limit equal to 285 A;
- Circuit B: overhead power line with a conductor section of 50 mm^2 and thermal limit equal to 230 A;

As evident in the following Sections, the method robustness guarantees no noticeable detrimental effects on the outcome's validity due to the above listed third-party field sources.

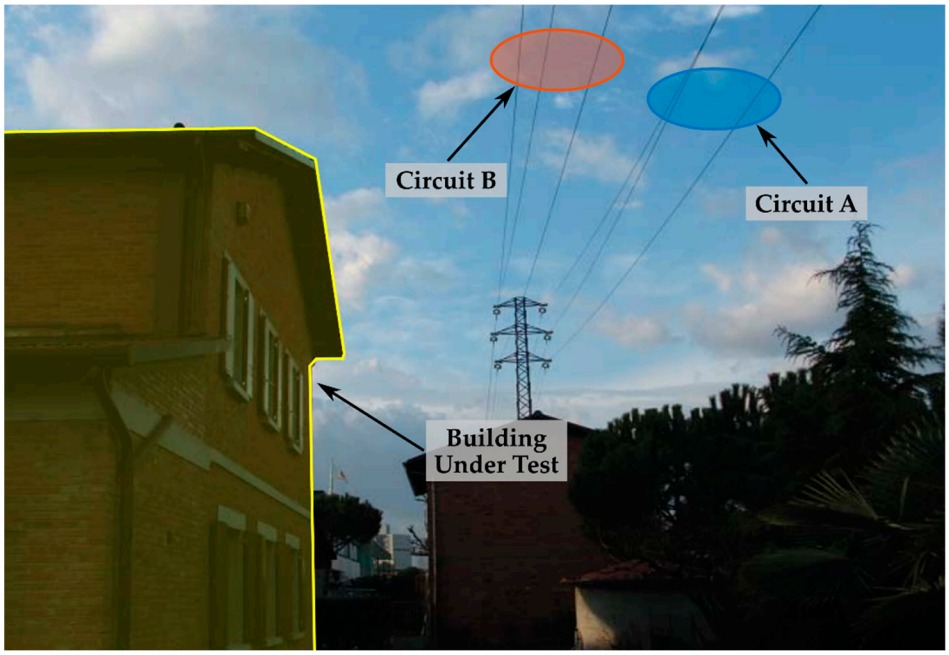

Figure 2. Building under test in front of the double-circuit medium voltage line.

4.2. Current Regulatory Framework

The area under consideration is located in the metropolitan area of Bologna, Italy, so the current laws regarding human exposure to magnetic fields generated by the power lines are the national and the regional ones of Emilia-Romagna. International exposure limits set by the International Commission on Non-Ionizing Radiation Protection (ICNIRP) are also considered. Below are briefly recalled the regulatory prescriptions assuming an industrial frequency of 50 Hz:

- Italian nationwide law: the Decree of The President of The Council of Ministers DPCM 8 July 2003 sets exposure limit to 100 μT, attention value 10 μT, and quality target 3 μT [12]. Concerning limits set by [12], measurement guidelines are reported in the CEI 106-11:2006 standard [32]. Occupational users' are regulated at the European level by 2013/35/EU [33];
- Emilia-Romagna law: although the region Emilia-Romagna is currently applying nationwide laws, in the first 2000s, magnetic field regulatory values for new buildings were set to an exposure limit of 100 μT, caution value 0.5 μT, and quality target 0.2 μT (similarly to what still applies in Brussels and Flanders area). Exposure values should be evaluated assuming I_r 5% higher than the average current experienced by the line in the previous year or, if more precautionary, 50% of the line rated current;
- ICNIRP limits: field values are set to 500 μT for occupational users' exposure and 100 μT for general public exposure [6];
- European Council recommendations: 1999/519/EC same as ICNIRP for the general public (100 μT) [6,11]. Occupational users' exposure set to 6 mT as for 2013/35/EU [33].
- IEEE and NATO recommendations: Head and torso should not overpass 904 μT and 2.71 mT in unrestricted and restricted environments, respectively. On the other hand, limb exposure is limited to 75.8 mT for all the environments. Further details are available in IEEE Std C95.1-2019 [14].

4.3. Description of the Measurement Procedure

The measurements were carried out during the 24 h of a winter working day considered to be well representative of normal operating conditions. The measured data was then processed numerically according to the previous Section's procedure to obtain the magnetic field's value corresponding to the reference current.

The measures were carried out following CEI 211-6:2001 standard (equitable to IEC 61786-2:2014) [34,35]. Due to the similar normative context, the reported conclusions also match IEC 62110:2009 and IEEE Std 644-2019 standards [36,37]. The measurement instrument is the PMM 8053 electromagnetic field meter, with a 50 Hz filter and isotropic probe EHP50B, mounted on wooden tripods, after preliminary calibration of the instrument. The adopted instrument is compliant with the IEC 61786-1:2013 and IEEE Std 1308-1994 [38,39].

As visible in Figure 3, the power line is with good approximation parallel to the North-West wall of the residential building under test. Therefore, the rooms most exposed to the magnetic field are those of the North-West side, foreground (building top floor, excluding the non-habitable attic). Indeed, among multiple spot measures carried out every short interval in various locations within the premises, the first-floor North-West side was the one experiencing the highest field values. If the building under test was not a residential space, [12] recommends verifying the exposure limits in the premises whose use is expected to be more than or equal to four hours per day. In other regional contexts (i.e., outside Italy), different reference exposure times may be applied.

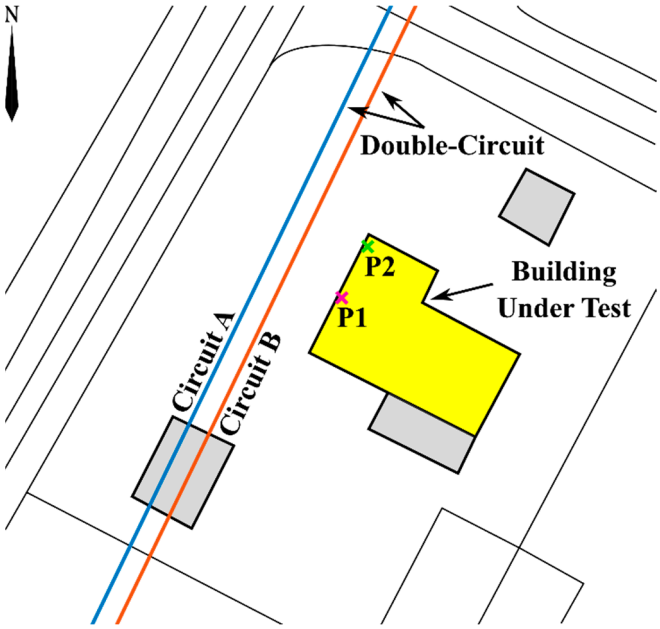

Figure 3. Cartographic representation of the building under test.

In particular, the preliminary instrumental survey identified two bedrooms on the first floor as particularly significant places for magnetic field exposure, as they are among the environments closest to the power line under consideration. Inside these two bedrooms, two measurement points were singled out close to the North-West wall (20 cm clearance) and at the top height (close to the ceiling). In Figure 3, these points are indicated as P1 (displayed in pink) and P2 (displayed in green) at the minimum distance from the overhead line. Although these points experience the maximum value of field (in the room), these are not the point where the maximum value of human exposure occurs. Actual human exposure should be tested by measuring the field at different elevations (same latitude and longitude), representing the human body dimension and activities more closely. Indeed, IEEE Std 644-2019 suggests a default position at an elevation of 1 m while IEC 62110:2009 proposes the so-called three-point measurement where the field is the arithmetic average between values sensed at 0.5 m, 1 m, and 1.5 m above the ground/floor [36,37]. On the other hand, D.L. n. 179/2012 prescribes measurement at 1.5 m above the floor (fields between 100 kHz and 300 GHz) [40]. Different contexts and regulatory bodies present various requirements. For the sole sake of the data collection, the above-described points were considered because the compliance of measured field values in these points

with laws/standards implies laws/standards compliance for all the other building areas and premises.

The measurement took place for 24-h on each point, and the field was sampled every 15 min. Figure 4 displays the measured field evolution in points P1 (pink trace) and P2 (green trace). Although the field measurement spanned over two different consecutive days, the proximity of points P1 and P2 ensure similar time evolution and cumulative distribution function (CDF) profiles. Statistical metrics reported in Table 1 support the latter statement. Therefore, the estimation of the coefficients is expected to provide similar values for the two positions.

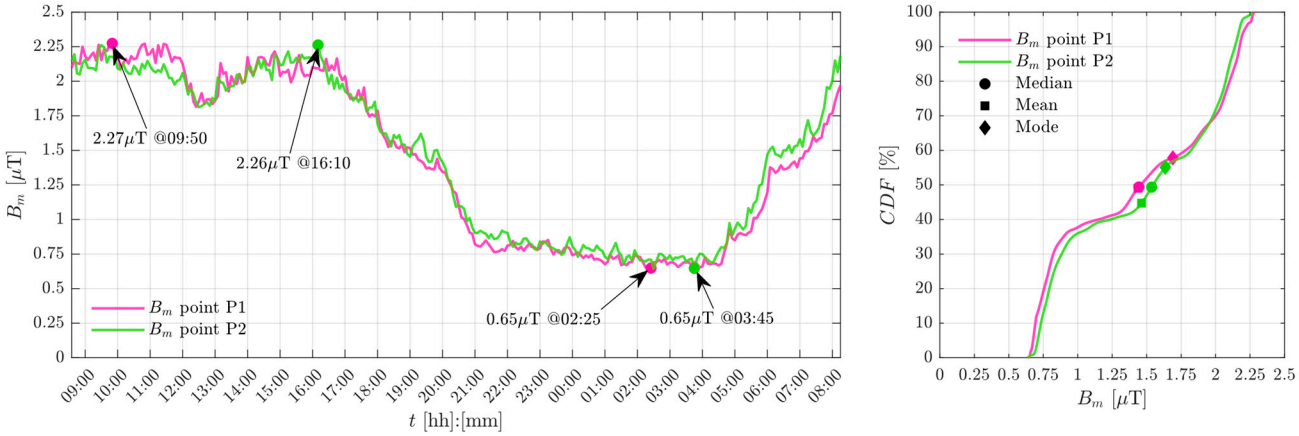

Figure 4. Measured field evolution over the 24 h (**left**) and its cumulative distribution function (**right**) for points P1 (pink trace) and P2 (green trace).

Table 1. Measured field statistics and information for points P1 and P2.

Point	Mean [μT]	Median [μT]	Mode [μT]	Min. [μT]	Max. [μT]	Starting Day
P1	1.44	1.44	1.69	0.65	2.27	23rd of January
P2	1.46	1.54	1.63	0.65	2.26	24th of January

In Figures 5 and 6, the instantaneous values of the currents in circuit A (blue traces) and circuit B (orange traces) over a 24-h span starting from the 23rd of January and 24th of January are displayed, respectively. As witnessed by the statistical metrics reported in Table 2 and by profiles in Figures 5 and 6, the two circuits are strongly unrelated. Therefore, the study of the field distribution with conventional methods is certainly not trivial. The two consecutive days present similar currents ensuring an alike level of significance.

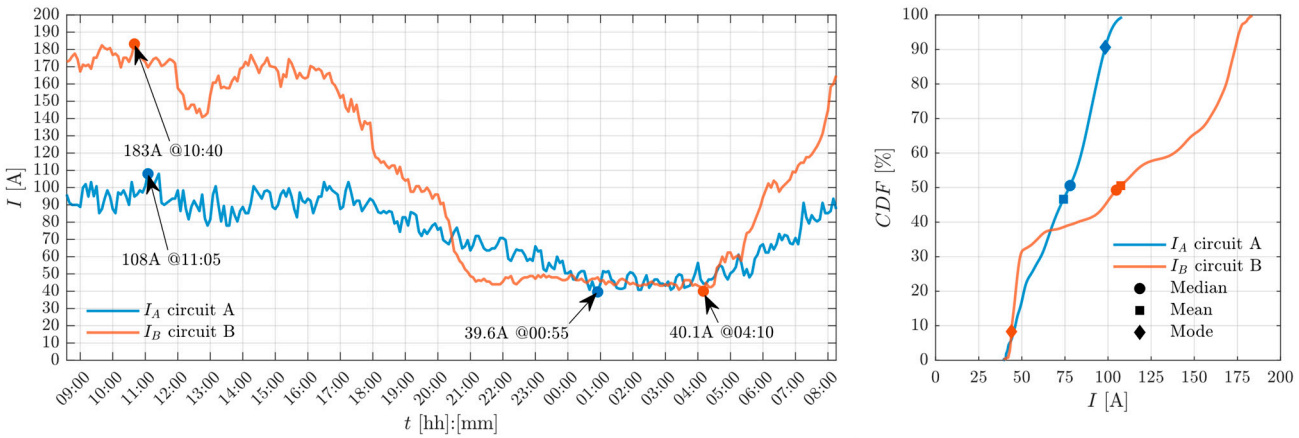

Figure 5. Instantaneous values of the currents over the 24 h (**left**) and its cumulative distribution function (**right**) in circuit A (blue trace) and circuit B (orange trace) starting from the 23rd of January.

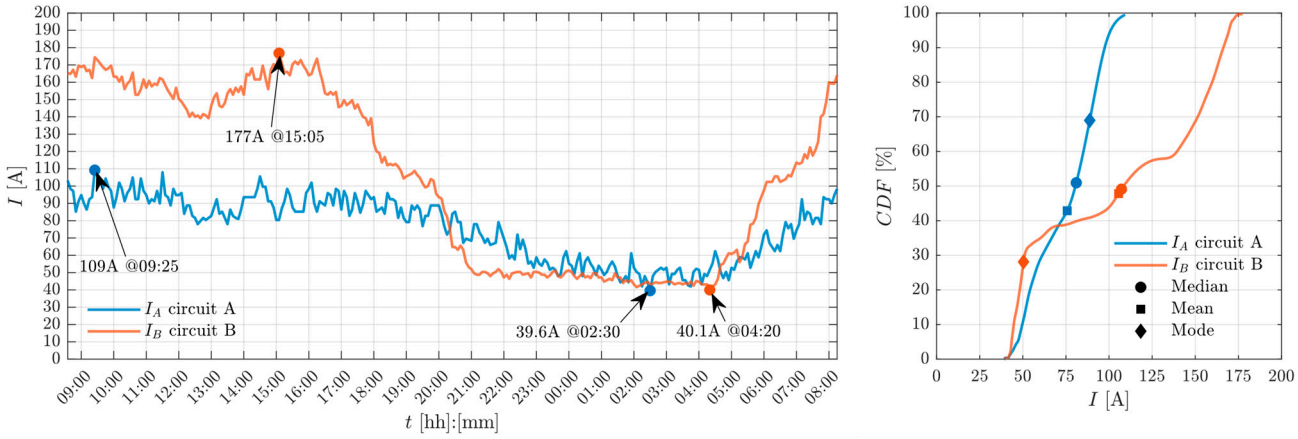

Figure 6. Instantaneous values of the currents over the 24 h (**left**) and its cumulative distribution function (**right**) in circuit A (blue trace) and circuit B (orange trace) starting from the 24th of January.

Table 2. Measured currents statistics and information for circuit A and circuit B.

Circuit	Mean [A]	Median [A]	Mode [A]	Min. [A]	Max. [A]	Starting Day
A	74.2	78.1	98.4	39.6	108	23rd of January
	75.7	81	88.8	39.6	109	24th of January
B	107	105	43.9	40.1	183	23rd of January
	106	107	50.4	40.1	177	24th of January

CDF profiles visible in Figures 4–6 are obtained from a kernel probability distribution function fitted using normal smoothing functions with a bandwidth equal to 0.1.

4.4. Measurements Processing Using the Proposed Procedure

Employing the multiple linear regression proposed in Section 3, proportionality coefficient estimation reported in Table 3 has been obtained. As argued above, since the two points are located at a similar distance from the line, remarkably similar coefficients have been obtained. Table 3 reports the 95% confidence interval for all the estimations. The resulting interpolating planes and acquired data are displayed in Figure 7 for points P1 (left) and P2 (right). As visible, minimal values of rms deviation (RMSD) and a determination coefficient (R^2) close to one witness the excellent grade of replication ensured by the model in both positions. The excellent matching between residuals standard deviation (σ) and RMSD testify the null error expected value. Finally, the high values of *F*-statistic and their associated *p*-value smaller than 0.05 show the statistical significance of the independent variables I_A and I_B in the prediction of the field.

Table 3. Proportionality coefficients estimation for points P1 and P2, their 95% confidence interval, and residual standard deviation.

Measurement Point	K_{PA} [μT/A]	95% Conf. Int. [μT/A]	K_{PB} [μT/A]	95% Conf. Int. [μT/A]	σ_ε [μT]
P1	0.0060	0.0060 ± 0.0003	0.0092	0.0092 ± 0.0002	0.052
P2	0.0060	0.0060 ± 0.0003	0.0095	0.0095 ± 0.0002	0.046

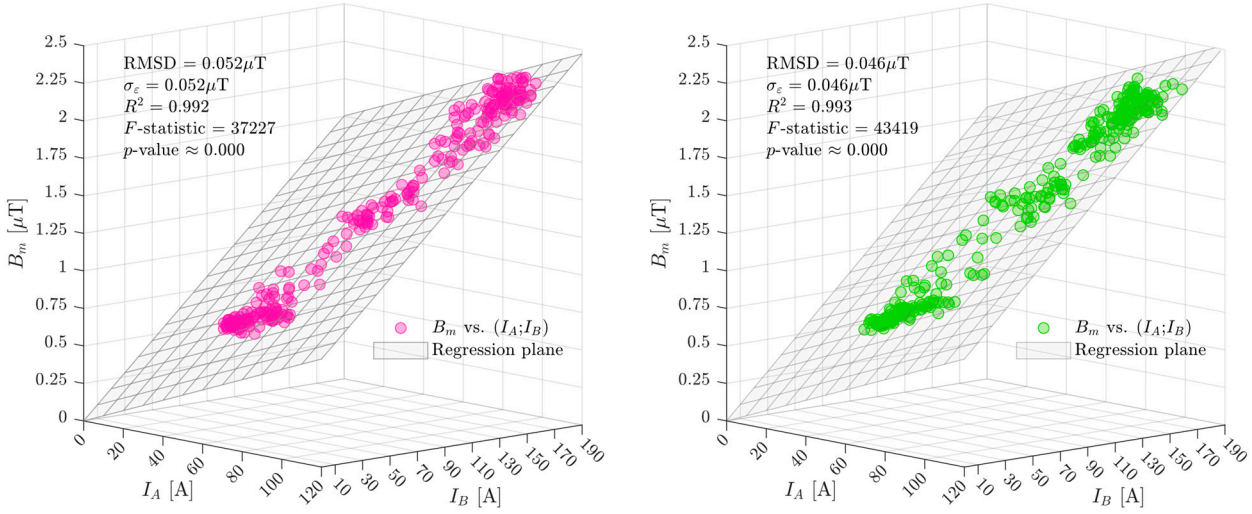

Figure 7. Regression planes together with acquired data for points P1 (**left**) and P2 (**right**).

Obtained values have been used for computing the calculated field B_c using Equation (18).

$$B_c = K_{PA} I_A + K_{PB} I_B \tag{18}$$

In Figure 8 calculated field (on the x-axis) has been compared with the measured one (on the y-axis) for points P1 (left) and P2 (right). Residuals absolute values versus measured field have been reported as well. Most—if not all—of the points are well located within the ±10% error boundary (gray areas) as visible in both cases. The same conclusion can be drawn from the histograms of the relative residuals (in %) and the associated Gaussian probability distribution functions (PDF, $\mathcal{N}$). For assessing the global behavior of the proposed technique, a linear fit has been carried out. For position P1 the slope differs from the ideal value by 6.2‰ while position P2 presents an error of about 1.6‰. RMSD and R^2 remain unchanged in comparison to Figure 7. Again, the residuals standard deviation (σ) presents a good match with the RMSD value. Indeed, the mean value of the percentage error distribution is only −0.45% and 0.53% for points P1 and P2, respectively. Finally, the Pearson coefficient (ρ) shows the particularly good linear correlation between calculated and measured values.

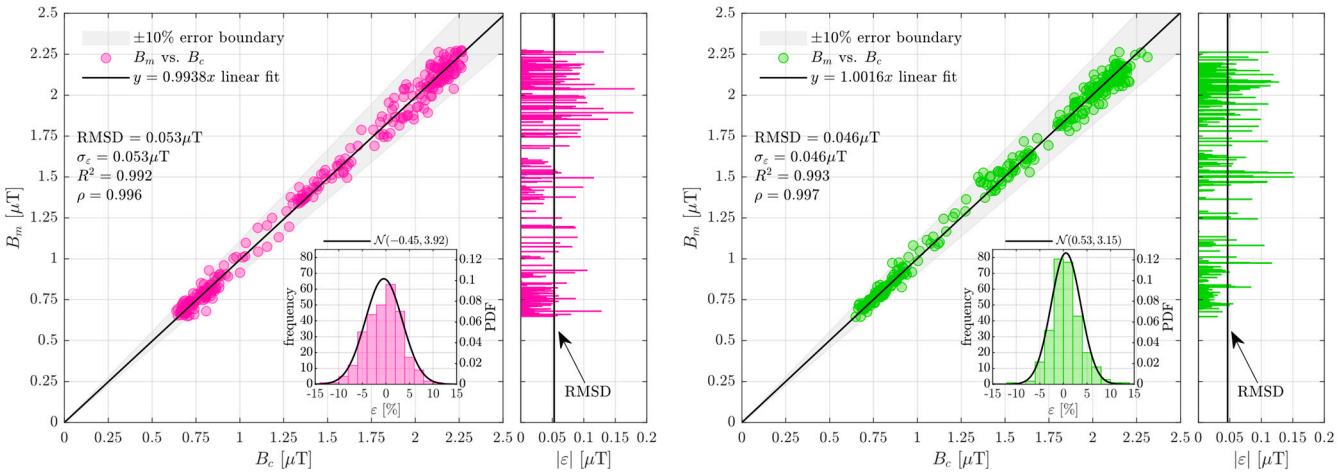

Figure 8. Proposed technique performance assessment for points P1 (**left**) and P2 (**right**).

As easily noticeable in Figures 9 and 10, the instantaneous measured field (solid lines) at points P1 and P2 is well bounded by the calculated field 95% confidence interval (filled

areas). The same conclusions can be drawn from the instantaneous residuals absolute value (solid red lines) adequately confined by the 95% confidence interval sideband (dash-dot lines). Furthermore, it can be derived that the showed confidence interval calculated using Equation (16) does not appreciably differ from the single value that σ_ε could have provided. Indeed, traces in Figures 9 and 10 settle around 107 nT and 96 nT while the more straightforward calculation $1.96 \cdot \sigma_\varepsilon$ produces 104 nT and 90 nT respectively for points P1 and P2.

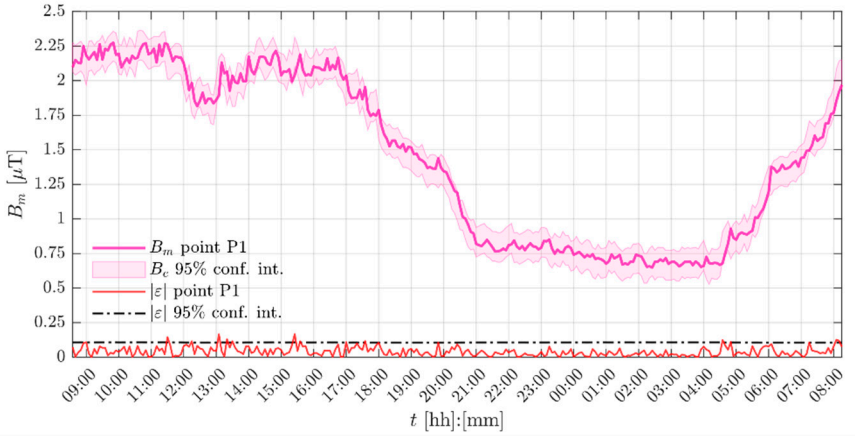

Figure 9. Position P1 measured field evolution over the 24 h (solid pink like) and its predicted 95% confidence interval (filled area). The absolute value of the residuals (red trace) is well confined by the confidence interval sideband (dash-dot line).

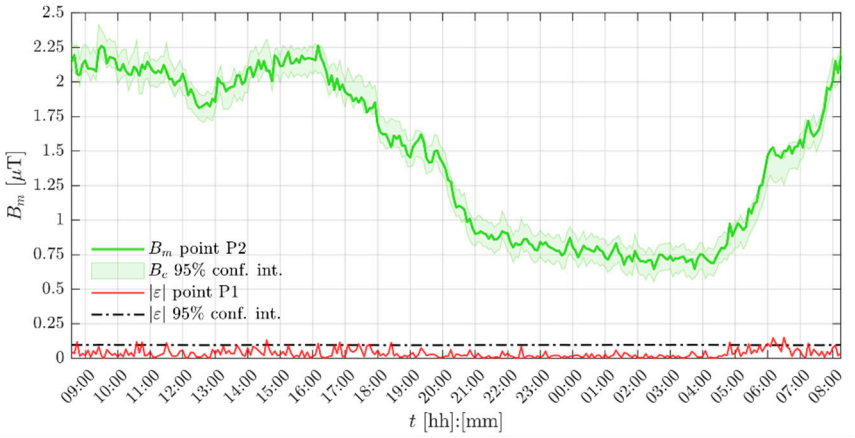

Figure 10. Position P2 measured field evolution over the 24 h (solid green like) and its predicted 95% confidence interval (filled area). The absolute value of the residuals (red trace) is well confined by the confidence interval sideband (dash-dot line).

4.5. Evaluation of the Magnetic Field Exposure

To evaluate the magnetic field exposure under various values of reference currents, two cases have been considered. Firstly B_R has been evaluated employing 50% of the line rated capacity; 142.5 A and 115.0 A for circuits A and B, respectively. Secondly, the maximum field value evaluated under 100% of the line rated current is provided. Finally, computed results are compared with the regulatory framework.

Computed data are collected in Table 4. As expected, points P1 and P2 exhibit comparable values in all the cases. Although the characterization in the two points has been performed with 24 h delay, the accuracy presents consistent values.

Table 4. Evaluation of magnetic field exposure for points P1 and P2.

Measurement Point	Load	I_{rA} [A]	I_{rB} [A]	B_R [μT]	95% Conf. Int. [μT]
P1	50%	142.5	115.0	1.92	1.92 ± 0.11
	100%	285.0	230.0	3.85	3.85 ± 0.14
P2	50%	142.5	115.0	1.95	1.95 ± 0.10
	100%	285.0	230.0	3.90	3.90 ± 0.13

It stands clear that reference values computed at 50% of the load appear more precautionary if compared to the median of the measurements reported in Table 1. In particular, without the proposed procedure, the field at point P1 would have been about 0.48 μT (−25%) smaller, while at point P2, the underestimation would have been about 0.41 μT (−21%). Even considering the lower confidence interval bound, these mismatches keep on being relevant. It can be noticed that at 100% of the load, the confidence intervals are wider (about +30%) if compared to the 50% case because the evaluated working point is farther away from the current sample means $(\overline{I}_A; \overline{I}_B)$.

The 100 μT exposure limit set by both nationwide codes and ICNIRP recommendations is well respected in all the cases. The attention value (10 μT) is overpassed neither in the case of standard load (50%) nor in the case of maximum current. While in the case of 100% load, the quality target (3 μT) is missed. If the Emilia-Romagna exposure limits were still in place, it would not have been possible to build the line (or the building) as in Figure 2 because both caution value (0.5 μT) and quality target (0.2 μT) would have been overpassed. These considerations are well visible in Figures 11 and 12, where Table 4 calculated points are plotted together with the current barycenter $(\overline{I}_A; \overline{I}_B)$. Field evolution (in μT) at the point P1 and P2 together with the quality target (3 μT) and its 95% confidence interval is displayed as well in the left column contour plot. The total standard deviation (in μT) is reported in the right column contour plot. As visible, far from the barycenter, the uncertainty starts ramping up noticeably.

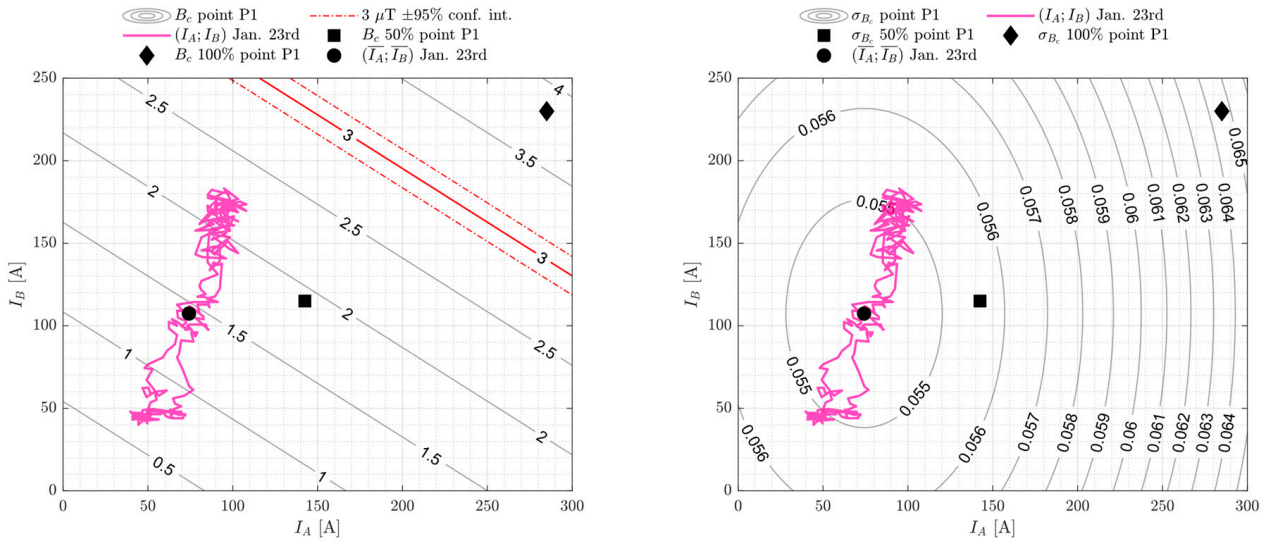

Figure 11. Positions P1 field (**left**) and its standard deviation (**right**) evolution (pink trace) over the 24 h as a function of the currents in circuits A and B (i.e., I_A and I_B). Current barycenter, and field evaluated at 50% and 100% of the line capacity are reported in all the frames.

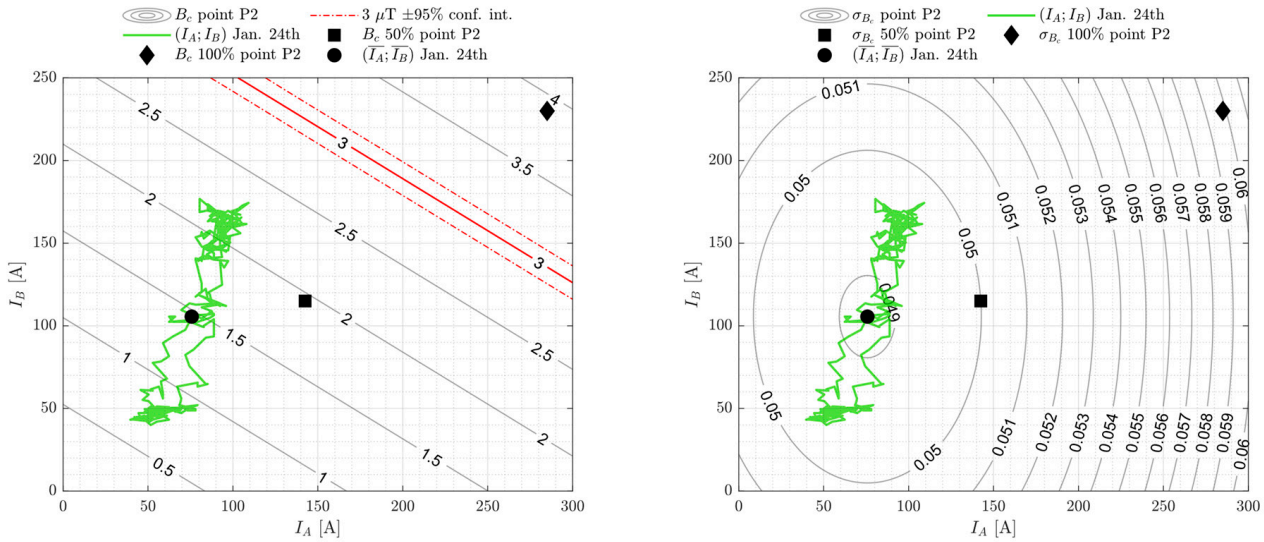

Figure 12. Positions P2 field (**left**) and its standard deviation (**right**) evolution (green trace) over the 24 h as a function of the currents in circuits A and B (i.e., I_A and I_B). Current barycenter, and field evaluated at 50% and 100% of the line capacity are reported in all the frames.

As anticipated, the method succeeds in providing field estimation for current reference values I_{rA} and I_{rB} that might be noticeably different from the set of data used for the regression. Third-party low-frequency field sources did not introduce any appreciable detrimental effects on the procedure. Since Section 2 assumptions and simplifications hold, no spatial information or 3D FEM codes was used at any development point (differently from the most state of the art).

5. Conclusions

This work described a straightforward methodology explicitly developed for non-optimized double-circuit medium-voltage overhead power lines. Using the multiple linear regression and the least mean squares techniques, it can estimate the proportionality coefficients between measured magnetic flux density and the line currents. The method has been thoroughly described with a particular focus on error assessment and accuracy interpretation.

The methodology has been successfully applied to an existing double-circuit line based on continuous measurement at peak field points and the acquisition of line load diagrams. The comparison of measurements with calculations has shown that, as assumed at the beginning of the validation procedure, at the two points of maximum exposure, the role of the other low-frequency sources was negligible and the estimation of the two proportionality coefficients allowed to determine the reference induction value in case of 50% and 100% of the standard maximum operating current. In all the cases, the technique provided outcomes with fair confidence intervals.

The current manuscript constitutes a good starting point for studying lines configurations like optimized double-circuit or multiple lines corridors here not treated. Future works might extend the presented approach considering third-party field sources and a more explicit accounting of measurement accuracy already at the regression level. Possible hints on these matters have been provided in the paper.

Author Contributions: Conceptualization, M.L., G.M., and R.M.; methodology, M.L., G.M., and R.M.; software, M.L. and R.M.; validation, M.L., G.M., and R.M.; formal analysis, M.L., G.M., and R.M.; investigation, M.L., G.M., and R.M.; resources, G.M. and R.M.; data curation, M.L., G.M., and R.M.; writing—original draft preparation, M.L., G.M., and R.M.; writing—review and editing, M.L., G.M., and R.M.; visualization, R.M. All authors have read and agreed to the published version of the manuscript.

Funding: This research received no external funding.

Institutional Review Board Statement: Not applicable.

Informed Consent Statement: Not applicable.

Data Availability Statement: Data is available in the paper.

Conflicts of Interest: The authors declare no conflict of interest.

References

1. Bendík, J.; Cenký, M.; Eleschová, Ž.; Beláň, A.; Cintula, B.; Janiga, P. Comparison of electromagnetic fields emitted by typical overhead power line towers. *Electr. Eng.* **2020**, 1–12. [CrossRef]
2. Woodside, G.; Kocurek, D.S. *Environmental, Safety, and Health Engineering*; Wiley: Hoboken, NJ, USA, 1997; ISBN 978-0-471-10932-7.
3. Olsen, R.G. *High Voltage Overhead Transmission Line Electromagnetics*; CreateSpace: Scotts Valley, CA, USA, 2018; Volume 2, ISBN 978-1507848043.
4. IARC. *Non-Ionizing Radiation, Part 1: Static and Extremely Low-frequency (ELF) Electric and Magnetic Fields*; IARC Publications: Lyon, France, 2002; ISBN 978-92-832-1280-6.
5. WHO. *Establishing a Dialogue on Risks from Electromagnetic Fields*; World Health Organization: Geneva, Switzerland, 2002.
6. International Commission on Non-Ionizing Radiation Protection. Guidelines for limiting exposure to time-varying electric, magnetic, and electromagnetic fields (up to 300 GHz). *Health Phys.* **1998**, *74*, 494–522.
7. CIGRE Working Group C3.19. *Responsible Management of Electric and Magnetic Fields (EMF)*; CIGRE Technical Brochure 806, Electra 311; CIGRE: Paris, France, 2020.
8. Tuominen, M.; Olsen, R. Electrical design parameters of all-dielectric-self-supporting fiber optic cable. *IEEE Trans. Power Deliv.* **2000**, *15*, 940–947. [CrossRef]
9. Schutt, A.J. The Power Line Dilemma: Compensation for Diminished Property Value Caused by Fear of Electromagnetic Fields. *Fla. State Univ. Law Rev.* **1996**, *24*, 125.
10. Stam, R. *Comparison of International Policies on Electromagnetic Fields*; National Institute of Public Health and Environment: Bilthoven, The Netherlands, 2018.
11. Publications Office of the EU. 1999/519/EC: Council Recommendation of 12 July 1999 on the Limitation of Exposure of the General Public to Electromagnetic Fields (0 Hz to 300 GHz). Available online: https://op.europa.eu/en/publication-detail/-/publication/9509b04f-1df0-4221-bfa2-c7af77975556/language-en (accessed on 20 May 2021).
12. Gazzetta Ufficiale Della Republica Italiana. DPCM 8 luglio 2003—Fissazione Dei Limiti DI Esposizione, Dei Valori DI Attenzione E Degli Obiettivi DI Qualità per la Protezione Della Popolazione Dalle Esposizioni AI Campi Elettrici E Magnetici Alla Frequenza DI Rete (50 Hz) Generati Dagli Elettrodotti. Available online: https://www.gazzettaufficiale.it/eli/id/2003/08/29/03A09749/sg (accessed on 18 May 2021). (In Italian)
13. Ranković, A. Novel multi-objective optimization method of electric and magnetic field emissions from double-circuit overhead power line. *Int. Trans. Electr. Energy Syst.* **2017**, *27*, 1–22. [CrossRef]
14. Institute of Electrical and Electronics Engineers. *IEEE Std C95.1-2019—IEEE Standard for Safety Levels with Respect to Human Exposure to Electric, Magnetic, and Electromagnetic Fields, 0 Hz to 300 GHz*; Institute of Electrical and Electronics Engineers: Piscataway, NJ, USA, 2019; pp. 1–312. [CrossRef]
15. Deltuva, R.; Lukočius, R. Distribution of Magnetic Field in 400 kV Double-Circuit Transmission Lines. *Appl. Sci.* **2020**, *10*, 3266. [CrossRef]
16. Mazzanti, G. The Role Played by Current Phase Shift on Magnetic Field Established by AC Double-Circuit Overhead Transmission Lines—Part I: Static Analysis. *IEEE Trans. Power Deliv.* **2006**, *21*, 939–948. [CrossRef]
17. Mazzanti, G. The Role Played by Current Phase Shift on Magnetic Field Established by Double-Circuit Overhead Transmission Lines—Part II: Dynamic Analysis. *IEEE Trans. Power Deliv.* **2006**, *21*, 949–958. [CrossRef]
18. Ponnle, A.; Adedeji, K.; Abe, B.; Jimoh, A. Spatial magnetic field polarization below balanced double-circuit linear configured power lines for six phase arrangements. In Proceedings of the 2015 Intl Aegean Conference on Electrical Machines Power Electronics (ACEMP), 2015 Intl Conference on Optimization of Electrical Electronic Equipment (OPTIM) 2015 Intl Symposium on Advanced Electromechanical Motion Systems (ELECTROMOTION), Side, Turkey, 2–4 September 2015; pp. 163–169.
19. Landini, M.; Mazzanti, G.; Sandrolini, L.; D'Adda, F. A Novel Algorithm for the 3D Calculation of the Magnetic Field Generated by Complex Configurations of Overhead Power Lines. In Proceedings of the 2019 IEEE International Conference on Environment and Electrical Engineering and 2019 IEEE Industrial and Commercial Power Systems Europe (EEEIC/I&CPS Europe), Genova, Italy, 11–14 June 2019; pp. 1–4.
20. Dahab, A.; Amoura, F.; Abu Elhaija, W. Comparison of Magnetic-Field Distribution of Noncompact and Compact Parallel Transmission-Line Configurations. *IEEE Trans. Power Deliv.* **2005**, *20*, 2114–2118. [CrossRef]
21. Khaled Omar Basharahil, M.; Azlinda Ahmad, N. Electromagnetic Fields Characteristics From Overhead Lines, Underground Cables and Transformers Determined Using Finite Element Method. In Proceedings of the 2021 IEEE International Conference on the Properties and Applications of Dielectric Materials (ICPADM), Johor Bahru, Malaysia, 12–14 July 2021; pp. 338–341.

22. Shiina, T.; Kudo, T.; Herai, D.; Kuranari, Y.; Sekiba, Y.; Yamazaki, K. Calculation of Internal Electric Fields Induced by Power Frequency Magnetic Fields During Live-Line Working Using Human Models With Realistic Postures. *IEEE Trans. Electromagn. Compat.* **2021**, 1–8. [CrossRef]
23. Lunca, E.; Istrate, M.; Salceanu, A.; Tibuliac, S. Computation of the magnetic field exposure from 110 kV overhead power lines. In Proceedings of the EPE 2012—Proceedings of the 2012 International Conference and Exposition on Electrical and Power Engineering, Iasi, Romania, 25–27 October 2012; pp. 628–631.
24. Mazzanti, G.; Landini, M.; Kandia, E. A Simple Innovative Method to Calculate the Magnetic Field Generated by Twisted Three-Phase Power Cables. *IEEE Trans. Power Deliv.* **2010**, *25*, 2646–2654. [CrossRef]
25. Mazzanti, G.; Landini, M.; Kandia, E.; Bernabei, A.; Cavallina, M. Magnetic Field Generated by Double-Circuit Twisted Three-Phase Cable Lines. *Prog. Electromagn. Res. C* **2017**, *73*, 115–126. [CrossRef]
26. Harun, Z.A.; Osman, M.; Ariffin, A.M.; Zainal Abidin Ab Kadir, M. Effect of AC Interference on HV Underground Cables Buried Within Transmission Lines Right of Way. In Proceedings of the 2021 IEEE International Conference on the Properties and Applications of Dielectric Materials (ICPADM), Johor Bahru, Malaysia, 12–14 July 2021; pp. 73–76.
27. SAI Global. CEI 211-4—Guide to Calculation Methods of Electric and Magnetic Fields Generated by Power-Lines and Electrical Substations. Available online: https://i2.saiglobal.com/management/display/anchor/346715/-/83253acef73050bb25f13edf9a274b1d (accessed on 18 April 2021).
28. ISO. ISO—17.220.20—Measurement of Electrical and Magnetic Quantities. Available online: https://www.iso.org/ics/17.220.20/x/ (accessed on 18 April 2021).
29. Mazzanti, G. Uncertainties in the calculation of continuous exposure of general public to magnetic field from ac overhead transmission lines. In Proceedings of the IEEE Power Engineering Society General Meeting, San Francisco, CA, USA, 16 June 2005; Volume 3, pp. 2583–2590.
30. Benes, M.; Comelli, M.; Bampo, A.; Villalta, R. Procedure di misura di campi elf in prossimità di configurazioni complesse di linee elettriche. In Proceedings of the AIRP—Convegno Nazionale di Radioprotezione, Catania, Italy, 15–17 September 2005; pp. 1–6.
31. Andreuccetti, D.; Zoppetti, N.; Fanelli, N.; Giorgi, A.; Rendina, R. Magnetic fields from overhead power lines: Advanced prediction techniques for environmental impact assessment and support to design. In Proceedings of the 2003 IEEE Bologna Power Tech Conference Proceedings, Bologna, Italy, 23–26 June 2003; Volume 2, pp. 1009–1015.
32. SAI Global. CEI 106-11—Guide for the Determination of the Respect Widths for Power Lines and Substations According to DPCM 8 July 2003 (Clause 6)—Part 1: Overhead Lines and Cables. Available online: https://i2.saiglobal.com/management/display/index/0/671694/-/79c654e525e1d90a0a4301ab29a3682f (accessed on 1 September 2021).
33. EUR-Lex. Directive 2013/35/EU of the European Parliament and of the Council of 26 June 2013 on the Minimum Health and Safety Requirements Regarding the Exposure of Workers to the Risks Arising from Physical Agents (Electromagnetic Fields) 20th Individual Directiv. Available online: https://eur-lex.europa.eu/legal-content/EN/TXT/?uri=CELEX%3A32013L0035 (accessed on 20 April 2021).
34. SAI Global. CEI 211-6—Guide for the Measurement and the Evaluation of Electric and Magnetic Fields in the Frequency Range 0 Hz–10 Khz, with Reference to the Human Exposure. Available online: https://eu.i2.saiglobal.com/management/display/index/0/346796/-/1aa8ad8d2af832b947bb25ee87e9204c (accessed on 18 April 2021).
35. SAI Global. IEC 61786-2:2014—Measurement of DC Magnetic, AC Magnetic and AC Electric Fields from 1 Hz to 100 kHz with Regard to Exposure of Human Beings—Part 2: Basic Standard for Measurements. Available online: https://webstore.iec.ch/publication/5907 (accessed on 1 September 2021).
36. SAI Global. IEC 62110:2009—Electric and Magnetic Field Levels Generated by AC Power Systems—Measurement Procedures with Regard to Public Exposure. Available online: https://webstore.iec.ch/publication/6473 (accessed on 25 August 2021).
37. IEEE Standards. *644-2019 (Revision IEEE Std 644-2008)—IEEE Standard Procedures for Measurement of Power Frequency Electric and Magnetic Fields from AC Power Lines*; IEEE Standards Association: Piscataway, NJ, USA, 2020; pp. 1–40. [CrossRef]
38. SAI Global. IEC 61786-1:2013—Measurement of DC Magnetic, AC Magnetic and AC Electric Fields from 1 Hz to 100 kHz with Regard to Exposure of Human Beings—Part 1: Requirements for Measuring Instruments. Available online: https://webstore.iec.ch/publication/5906 (accessed on 1 September 2021).
39. IEEE Standards. *1308-1994—IEEE Recommended Practice for Instrumentation: Specifications for Magnetic Flux Density and Electric Field Strength Meters—10 Hz to 3 kHz*; IEEE Standards Association: Piscataway, NJ, USA, 2020. [CrossRef]
40. Gazzetta Ufficiale Della Republica Italiana. D.L. 18 Ottobre 2012, N. 179—Ulteriori Misure Urgenti per la Crescita Del Paese. Available online: https://www.gazzettaufficiale.it/eli/gu/2012/12/18/294/so/208/sg/pdf (accessed on 28 August 2021). (In Italian)